Fast and Accurate Iron Loss Evaluation Using Static FEA for Traction PMSMs

Fast and Accurate Iron Loss Evaluation Using Static FEA for Traction PMSMs

Paolo Ragazzo
Dipartimento Energia Galileo Ferraris
Politecnico di Torino
Turin, Italy
paolo.ragazzo@polito.it

Gaetano Dilevrano
Dipartimento Energia Galileo Ferraris
Politecnico di Torino
Turin, Italy
gaetano.dilevrano@polito.it

Simone Ferrari
Dipartimento Energia Galileo Ferraris
Politecnico di Torino
Turin, Italy
simone.ferrari@polito.it

Gianmario Pellegrino
Dipartimento Energia Galileo Ferraris
Politecnico di Torino
Turin, Italy
gianmario.pellegrino@polito.it

***Abstract*—This paper delves into the accurate evaluation of iron loss in permanent magnet synchronous machines, with special emphasis on traction applications. First, iron loss models from the literature are comparatively assessed based on the criteria of their effectiveness and accessibility in terms of required steel data. The primary challenges associated with iron loss modelling through finite-element analysis are outlined; namely, they are the detection of minor and major hysteresis loops, with appropriate accounting of DC flux density bias, mechanical stress and PWM supply effects. In the second part of the paper, the novel approach called Augmented iGSE is introduced, inspired to the improved Generalized Steinmetz's Equation. This model is obtained by combining the strengths of the best models found in the literature. Also, solutions for time minimization are exposed. The outcome is an iron loss model that excels in its ability to comprehensively model every relevant phenomenon by using a simple magnetostatic solver and a set of iron data based on common measurements provided by electrical steel manufacturers.**

***Index Terms*—permanent magnet synchronous machines, iron loss, static simulation**

I. Introduction

A. Background

Iron core losses arise due to time variation of the magnetic field in the stator and the rotor of electrical machines [1]. The two physical mechanisms that produce iron losses are hysteresis loops and eddy currents. Hysteresis losses are closely associated with the magnetic properties of silicon iron [2]. When magnetic excitation is successively increased and decreased, the resulting flux density does not follow a reversible path but exhibits a hysteresis effect, as shown in Fig. 1. Eddy currents are also induced by variations of the magnetic field. According to Faraday's law, an electromotive force is generated in a conductor when it is exposed to a magnetic flux changing over time. Consequently, a current circulates within the conductor, forming closed loops perpendicular to the magnetic field lines. Therefore, this eddy current produces Joule loss and a magnetic reaction field. Modelling eddy currents can be approached by visualizing them as a hysteresis curve that widens proportionally with frequency, similar to an increase in magnetic coercivity [3].

B. Scope of the paper

The paper provides a comprehensive review of iron loss modelling, specifically addressing the key challenges relevant to, and not only to, automotive applications. It focuses on critical physical phenomena such as major and minor hysteresis loops, DC flux density bias, mechanical stress effect, and PWM supply. The models existing in the literature are evaluated in terms of their capability to capture these phenomena, revealing the lack of a comprehensive model.
In response to this gap, the paper proposes a novel model that considers all the mentioned phenomena, leveraging on a freeware magnetostatic solver. Time minimization techniques are introduced to enhance the efficiency of the proposed model. The methodology is illustrated with reference to a permanent magnet synchronous machine (PMSM) designed for automotive traction application, specifically an interior-

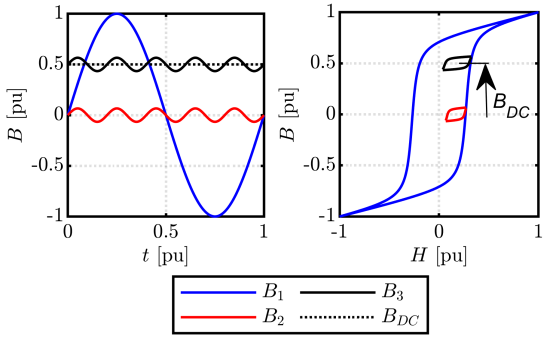

Fig. 1. Flux density waveforms tracing the major (blue) and minor (red and black) hysteresis loops.

PM motor designed on the active dimensions and output specifications of the Tesla Model 3 3D5 motor. Comparative analyses of results and computational times are conducted against the transient commercial FEA solver Ansys Maxwell, highlighting the value and effectiveness of the proposed model. In particular, the analysis of losses under PWM supply is conducted utilizing an automatically generated circuital model of the PMSM drive to evaluate the steady-state PWM current waveforms under closed-loop vector control, and then running the magnetostatic FEA under the so obtained nonsinusoidal current waveforms. In contrast, commercial software address this task using co-simulation, i.e. integrating the dynamic circuital model and the transient FEA solver.

II. Challenges on the iron loss model for PMSM

Traction OEMs and TIER 1 companies aim at continuously increasing the efficiency and compactness of electrified drivetrains; indeed, the iron losses of the traction e-motor are the higher loss contribution of the motor after copper losses, and have a significant impact on the machine- and drivetrain overall efficiency especially at high-speed and at partial load conditions. Even before efficiency concerns, the accurate determination of iron losses is of paramount importance for thermal management optimization in the twofold perspective of e-motor volume reduction and respecting its thermal limits. Despite the historical effort of the scientific community, the iron loss estimation is still cumbersome and frequently imprecise, so much so different design processes rely on loss correction factors as large as 1.5 to 2 with respect to the estimated losses. Currently, multiple iron loss models coexist and the community has not defined an ultimate one of general use. The main sources of uncertainty in iron loss estimation are:

- complex modelling - iron losses are caused by convoluted physical phenomena that are not easy to model even with FEA. Among these, in the following, the presence of both major and minor hysteresis loops is highlighted as well as the impact of the DC bias on the flux density (i.e. minor loops distortion).
- multiple factors in play - among these, steel manufacturing, mechanical stress and inverter modulation significantly affect the iron loss outcome.
- poor data - still today, silicon-iron loss data are provided in a form initially meant for transformers, based on sinusoidal excitation in a single direction, according to the Epstein's frame standard test [4].

A. Iron loss models comparative overview

Over the last century, several iron loss models have been developed, with increasing degrees of accuracy and complexity. Actually, there is not a champion model overcoming the others in every aspect. In [5], 10 iron loss models are compared with experimental findings; according to the authors, every presented technique seems to excel in modelling specific phenomena, but no one is capable of accurately modelling everything, and no preferred approach is clearly addressed.

TABLE I
Comparison of iron loss computation methods

	Minor loops	DC bias	Mech stress	Material data
Steinmetz	No	No	No	Low
MSE	Yes	No	No	Low
GSE	No	Yes	No	Low
iGSE	Yes	No	No	Low
Bertotti	No	No	No	Low
Δ Bertotti	Yes	Yes	No	Low
Jiles-Atherton	Yes	Yes	No	High
Hysteresis FEA	Yes	Yes	Yes	Medium

Tab. I highlights whether an iron model is capable of capturing the minor loops, DC bias and mechanical stress impacts. Also, the ease of use, intended as the required level of knowledge to run the model, is graded. If the requested material knowledge is low, it means that the standard iron loss curves are enough to support the model, whilst medium and high levels require specific and advanced measurements on the iron sheets.
At the end of the 19^{th} century, C. P. Steinmetz [2] proposed an iron loss modelling that turned into a milestone: the specific iron losses p_{Fe} (W/kg) in a magnetic material are a function of flux density B and its frequency f. Here we refer to the two-term variant of the original Steinmetz equation (1).

$$p_{Fe} = k_{SE,h} \cdot f^{\alpha} B^{\beta} + k_{SE,e} \cdot (fB)^2 \tag{1}$$

Where the three coefficients $k_{SE,h}$, $k_{SE,e}$, α and β are obtained by fitting the measured loss data provided by the steel manufacturer. Concerning the Steinmetz-based models, the classical [2] is the weakest but it envisioned the subsequent models [6] [7] that achieved to contemplate either the minor loops or the DC bias, although not both in the same model. The Steinmetz models benefit from simple inputs, that are commonly found in the standard data provided by manufacturers. Like, the classical Steinmetz model, also the initial Bertotti equation is fragile [1], but posterior versions are more powerful, as the differential Bertotti [8] (indicated as Δ Bertotti) used in Ansys Maxwell; yet, it is valid only with transient FEA. On the other hand, Jiles-Atherton [3] is accurate but it is a complex model based on manifold coefficients with cumbersome retrievement. Last, the FEA that models the iron with a hysteresis loop and not with a characteristic BH curve are the most powerful but few solvers support it [9].

B. Major and minor hysteresis loops

Considering the three-phase stator windings set of a PMSM supplied with purely sinusoidal currents, and neglecting the effect of harmonic fields produced by anisotropy and saturation, the stator iron tends to show sinusoidal flux density waveforms in the x-y dimensions of its cross-section. Conversely, as the rotor rotates synchronously with the rotating magnetic field, its iron core sees a flux density field of constant amplitude over time.
According to the mentioned assumptions, in Fig. 1, the blue curve is an example of what generally happens in one point of a stator tooth. The sinusoidal flux density at the fundamental

frequency B_1 traces the blue major hysteresis loop. Equivalently, the constant value B_{DC} represents the ideal behaviour of a generic point in the rotor. However, even under sinusoidal excitation, higher order harmonic fields appear in the iron, given for example by the alternated rotor permeance values at the airgap, as seen by the considered stator tooth, and the stator/slot permeance modulation, as seen from the rotor. Such higher-order harmonics add to the ideal sinusoidal and constant flux density trends in the stator and the rotor respectively, creating corresponding minor hysteresis loops (e.g. the red and black curve in Fig. 1). The resulting total iron losses consist of the traced area of both major and minor loops, and detecting every minor loop is a major challenge for accurate iron loss modelling.

C. DC bias on flux density waveforms

The area enclosed by a minor hysteresis loop depends on the peak to peak flux density amplitude but also on the DC offset B_{DC}, as defined in Fig. 1. The impact of DC offset on loss is notable in Fig. 1, where although the black and red minor loops have the same pk-pk amplitude, yet the one with DC offset covers a visibly larger area.
Overall, the work [10] claims to reach the best compromise between accuracy and ease of use: starting from the general equation (2), the final model (α=0.65, λ=2.1) is found by fitting measurements on six steel grades commonly used for electrical machines.

$$k_{Fe,DC} = \alpha B_{DC}^{\lambda} + 1 \tag{2}$$

$k_{Fe,DC}$ is the loss increment factor due to B_{DC}, while α and λ are empirical coefficients found to be around 0.65 and 2.1, respectively, for the six tested steels. Graphically, the relationship (2) can be visualized as in Fig. 2a.

D. Impact of mechanical stress

Notably, the magnetic properties of electrical steel sheets are influenced by mechanical stress [11]. Indeed, whenever a ferromagnetic material is subject to a variable magnetic field, it endures a change in dimension according to magnetostriction. An applied mechanical stress due to other factors (e.g. centrifugal forces in the rotor or the housing pressure on the stator) alters the magnetostrictive behaviour and causes a variation in the magnetic performance and the hysteresis loss characteristics, while eddy currents are unchanged.
During the last decade, Yamazaki et al. investigated the impact of mechanical stress on the core magnetic characteristics: in [12], the formulation (3) is proposed to model the compressive stress effect on the iron loss, while the tensile stress impact is neglected (i.e. increment factor equal to 1). Therefore, the model (3) is suitable to compute the stress impact on the stator, where the stress is compressive due to shrink-fitting into the housing, but not on the rotor.

$$k_{Fe,mech} = 1 + (C_{h,max} - 1)e^{-\frac{B}{B_h}} \cdot (1 - e^{-\frac{|\sigma|}{\sigma_h}}) \tag{3}$$

The coefficients $C_{h,max}$, B_h and σ_h describe the loss variation with flux density and stress; they were retrieved by experiments on the studied core ($C_{h,max}$ = 4.9, B_h = 0.7 T and σ_h = 100 MPa).
By graphically plotting (3) in Fig. 2b, it is evident that the stress impact is magnified at low flux density, while it tends to be negligible towards high flux density values. Notably, several stages in the manufacturing process can introduce further mechanical stress in the iron core [13]. For instance, the cutting process influences the material properties due to uneven stress, therefore, the losses on small-size machines are more influenced by the cutting quality since the cut edges account for a larger portion of the total iron volume.

E. Impact of the inverter supply

A multitude of studies in the literature highlights the impact of the inverter supply on iron loss [9]. Indeed, shifting from an ideal sinusoidal supply can significantly change the amount of iron loss: the high-frequency time harmonics of the supply induce high-frequency fields in the core creating additional losses. In particular, the phase current ripple causes high-frequency minor hysteresis loops, whose loss contribution is magnified by the flux density DC offset produced by the fundamental component of the magnetic field. The influence of the PWM supply on PM eddy current loss is even more pronounced [14]. Therefore, contemplating the inverter supply impact on iron (and PM) loss is mandatory in the design process to properly estimate the thermal response of the machine and its efficiency. Increasing the switching frequency can be advantageous for the motor loss, but the drive is penalized inverter side [15].

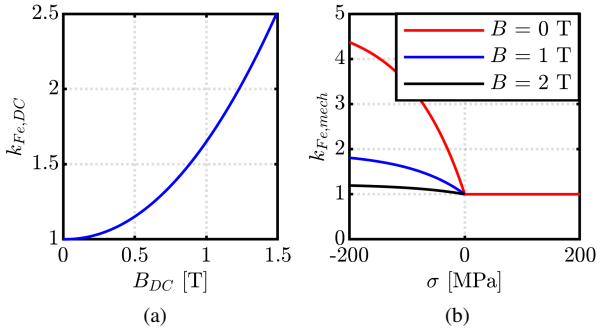

Fig. 2. (a) Iron loss increment factor $k_{Fe,DC}$ due to DC-bias on the flux density B_{DC}. (b) Iron loss increment factor $k_{Fe,mech}$ due to mechanical stress σ.

III. Augmented iGSE model

In this manuscript, the proposed iron loss model is based on the improved Generalized Steinmetz Equation (iGSE) [7] [16] with add-ons to contemplate the DC bias effect and the stator mechanical stress due to shrink-fitting. As underlined by the comparing Tab. I, despite its excellent ease of use, the original iGSE do not model the mentioned effects. Therefore, the adjustment factors introduced in Sec. II are applied to empower the original iGSE. The eddy current iron loss are computed as detailed in [16].

A. Minor and major loops detection

Firstly, the original iGSE [7] is applied via MATLAB scripting to the FEMM field solution to retrieve the iron loss of each mesh element. The iGSE computation is based on the formulation (4). Note that (4) is valid for every hysteresis loop, both minor and major.

$$p_{Fe,iGSE} = \frac{1}{T}\int_0^T k_{iGSE}\left|\frac{dB}{dt}\right|^{\alpha}(\Delta B)^{\beta-\alpha}dt \tag{4}$$

Where ΔB is the peak-to-peak flux density of the considered loop and the k_{iGSE} is retrieved by the Steinmetz coefficient as (5), which are calculated by fitting the manufacturer loss curves.

$$k_{iGSE} = \frac{k_{SE}}{(2\pi)^{\alpha-1}\int_0^{2\pi}|\cos\theta|^{\alpha}\,2^{\beta-\alpha}d\theta} \tag{5}$$

Where θ is the angular position in electrical degrees. The iGSE elaborates on the flux density waveforms, their features are briefly summarized in the following.

Besides, the iGSE algorithm receives a non-sinusoidal flux density waveform from FEMM and it discerns the major and minor loops. This is done by partitioning the waveform into two sections, a rising and a falling one, and thus the start of a minor loop is detected as a change in the slope of the waveform [7]. The identified minor loop ends when the flux density reaches the initial value, namely at the minor loop start. Note that also nested levels of minor loops can be detected. Thus, once the minor loops are spotted, they are detached from the main waveform to obtain the major loop.

B. Additional loss due to DC bias and compressive stress

Once the iron losses for each mesh element and hysteresis loop are computed according to the original iGSE ($p_{Fe,iGSE}$), adjustments are applied to contemplate the minor loop enlargement due to the flux density DC bias as well as the compressive stress produced by the shrink fitting, as in (6).

$$p_{Fe} = k_{Fe,DC}\cdot k_{Fe,mech}\cdot p_{Fe,iGSE} \tag{6}$$

Thus, the loss of every loop and of every mesh are summed to retrieve the total loss. The DC bias is accounted for with an increment factor $k_{Fe,DC}$ proportional to B_{DC} (2). Notably, the B_{DC} is calculated for each loop from the FEA field solution, thus, the $k_{Fe,DC}$ computation does not need any additional information on the iron sheets, since the classical Steinmetz coefficients are sufficient to run the analysis.

Subsequently, the compressive stress on the stator is accounted for with the increment factor $k_{Fe,mech}$, defined as in (3). It depends not only on the B field solution but also on the mechanical stress. Therefore, to take the mechanical stress into account, the expected stress must be inserted by the user according to the adopted technique during the assembly process [13]. Thus, the peak stress occurs at the contact point with the housing and it gradually diminishes towards the rotor [17]. However, the discussed analysis simplifies the problem by assuming a singular and uniform value for the stator iron. The consistent impact of both these adjustments on the loss results is reported in Sec.IV.

C. Computational time minimization

To minimize the computational time of an iron loss simulation in a single (i_d,i_q) or torque operating point at a defined speed, parallel computing and symmetry can be exploited. Firstly, note that the adopted iron loss computation requires a complete flux density waveform, namely an electric period. The number of steps within the 360 electrical degrees is flexible and must be chosen according to the target maximum loss harmonic, as disclosed later in this section.

Before the time minimization, it took **106 minutes** to run a single point iron loss simulation under sinusoidal supply by using the reference workstation (Intel Xeon E5-2690 v4, 14 cores and 32GB) and 360 rotor positions over one electrical period.

However, by exploiting the half-period symmetry on the flux density waveforms, the computation time is easily halved, since half of the period can be simulated while the other half of the waveform can be reconstructed by mirroring the first part, thanks to the odd symmetry of field quantities. This nature can be appreciated in Fig. 3 and it is valid for every mesh element. The computation time is thus reduced from 106 to 53 minutes.

Concerning parallel computing, note that considering a magnetostatic simulation, the solution of a specific instant (rotor position) is independent of the solution of a different instant. Therefore, the whole angular span of 180° can be sliced among the computer cores. Namely, given a number of cores n_{core}, each core will cover an angular span $\Delta\theta_{core}$ equal to:

$$\Delta\theta_{core} = \frac{180°}{n_{core}} \tag{7}$$

This allows a substantial reduction of computational time. For example, by exploiting 8 cores, the computational time is reduced from 53 to **9 minutes**. A single-point simulation with similar mesh and same number of rotor steps using the transient solver of Ansys Maxwell takes around 11 minutes, using a single core. Fig. 4 reports the computational time function of the number of cores working in parallel. Notably, considering the utilised workstation, no time reduction is registered by moving from 12 to 14 working cores, indeed

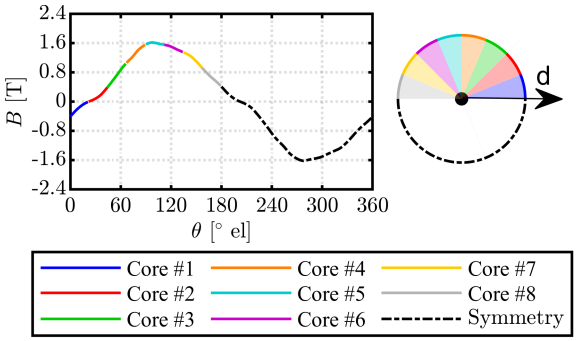

Fig. 3. Illustration on how the angular span is split among the cores (example refers to eight cores). The portion of the waveform retrieved by symmetry is highlighted with dots.

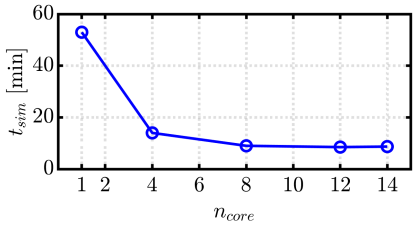

Fig. 4. Computational time of a single-point iron loss computation as a function of the number of cores working in parallel.

the 12 cores simulation reaches the minimum computational time. Note that the discussed parallelization is employed for the single-point analysis: for loss map evaluation the default procedure is using one core per i_{dq} operating point.
It is important to note that the simulation setup employed in this example (180 steps on 180 electrical degrees) captures spatial harmonics under sinusoidal supply but it is not enough fine-grained for PWM supply. For a comprehensive PWM loss analysis, a minimum of 10 samples per time harmonic of interest is recommended. For instance, using a switching frequency of 10kHz with this 6-pole PMSM at 4000rpm the number of recommended rotor steps is 500, corresponding to 10 samples across 50μs (twice the switching frequency). In this case the simulation would take 12.5 minutes. Note that the PWM simulation time depends on the ratio between fundamental frequency (speed) and switching frequency: lower speed value will require more rotor steps, increasing the computational burden, and vice-versa.

IV. Case Study

In the following, example results are provided based on a V-shape PMSM traction motor resembling the motor mounted on the Tesla Model 3 3D5. The radial cross-section of the benchmark motor is displayed in Fig. 5 and its ratings are reported in Tab. II.

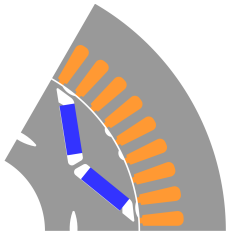

Fig. 5. Radial cross-section of the Tesla Model 3 PMSM.

TABLE II
Tesla Model 3 3D5 ratings

Max current	I_{max}	1414	[Apk]
Max torque	T_{max}	430	[Nm]
Min DC-link voltage	V_{dc}	231	[V]
Max speed	n_{max}	18100	[rpm]
Max power	P_{max}	192	[kW]

A. Single point evaluation

To highlight the impact of the adjustment factors with respect to the original iGSE, a single point, reported as a black dot in Fig. 7b, is investigated with sinusoidal and non-sinusoidal supplies: 700Apk (half the maximum current) in MTPA with a rotor speed of 4000 rpm, producing around 230Nm.

Fig. 6 reports the stator and rotor iron losses of the studied operating point with three different algorithms under sinusoidal supply: the original iGSE [7], iGSE augmented with the DC bias effect and iGSE with both DC bias and mechanical stress effects. A compressive stress of -100MPa is considered. Notably, the DC bias affects the stator losses more than rotor losses; this happens because the DC bias amplifies only the hysteresis loss, representing a minor contribution compared to the eddy currents loss in the rotor. Then, in Fig. 6, the results of Ansys Maxwell are also reported. Note that, the FEMM and Ansys Maxwell models have comparable mesh and the same number of rotor steps.
In Fig. 6, the impact of PWM supply is demonstrated in the same operating point. The non-sinusoidal current waveforms are obtained through a circuital model integrated into SyR-e, known as syreDrive [18]. These waveforms are then used to conduct a FEA that is post-processed with the augmented iGSE computation. A surge in losses of approximately 33% is observed, and this finding is corroborated by similar results obtained in Ansys Maxwell. Overall, the stator loss increases due to $k_{Fe,DC}$ and $k_{Fe,mech}$ are respectively equal to 45% and 30%, therefore a 90% loss hike with respect to the original iGSE estimation. Nonetheless, the exact compressive stress value is complex to forecast at the design stage since depends on the assembly process. To better assess its potential impact, Fig. 7a shows the stator iron losses as a function of the compressive stress, revealing a maximum iron losses

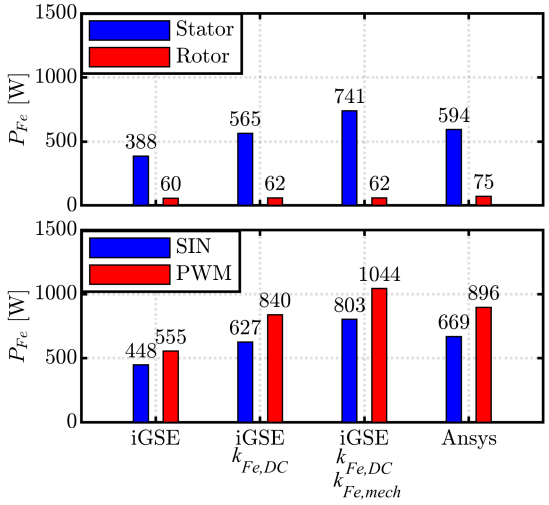

Fig. 6. Iron loss results at 230 Nm and 4000 rpm: discussed methods vs Ansys Maxwell. Top chart: stator and rotor losses breakdown under sinusoidal supply; bottom: comparison between sinusoidal and PWM supply.

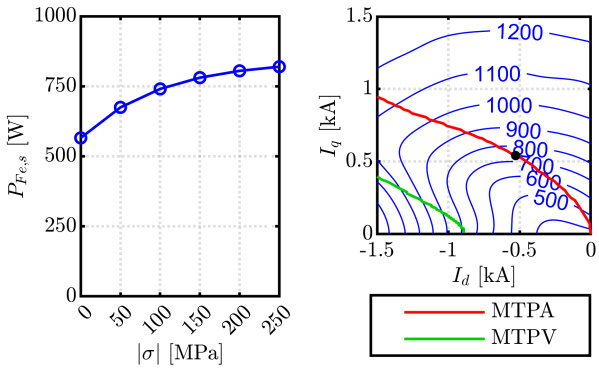

(a) (b)

Fig. 7. (a) Stator iron loss function compressive mechanical stress. (b) Iron loss contours over the i_{dq} plane for Θ_{PM} = 80°C at 4000rpm and sinusoidal supply; the 230Nm operating point is highlighted with a black marker.

boost equal to 45%.

B. Loss map

Finally, the iron loss map across the dq current domain can be determined by simulating a current grid domain under sinusoidal supply, as shown in Fig. 7b. This is speed-scaled without re-simulation using the frequency exponents of the loss law (1) as elaborated in [16].

V. Conclusion

This paper explores the challenges associated with iron loss evaluation in PMSMs designed for traction. Through a critical assessment of various prevalent iron loss models, it becomes evident that there is an absence of a comprehensive and straightforward model. The paper introduces an Advanced iGSE iron loss model approach considering specific add-ons. The result is an accurate iron loss computation technique based on magnetostatic FEA simulations, showing comparable accuracy and to leading software such as Ansys Maxwell and good computational efficiency. Notably, the proposed algorithm extends its utility by quantifying the impact of compressive stress on the stator. This procedure proves its versatility, enabling iron loss mapping also under PWM supply conditions. In essence, the presented methodology addresses existing challenges in iron loss modelling and offers a practical and open-access calculation tool for iron loss evaluation.

Acknowledgment

The research has been conducted with the support of Power Electronics Innovation Center (PEIC) of Politecnico di Torino.

References

[1] G. Bertotti, "General properties of power losses in soft ferromagnetic materials," *IEEE Transactions on Magnetics*, vol. 24, no. 1, pp. 621–630, Jan. 1988.

[2] C. P. Steinmetz, "On the Law of Hysteresis," *Transactions of the American Institute of Electrical Engineers*, vol. IX, no. 1, pp. 1–64, Jan. 1892.

[3] D. C. Jiles and D. L. Atherton, "Theory of ferromagnetic hysteresis," *Journal of Magnetism and Magnetic Materials*, vol. 61, no. 1, pp. 48–60, Sep. 1986.

[4] *Magnetic materials – Part 2: Methods of measurement of the magnetic properties of electrical steel strip and sheet by means of an Epstein frame*, ser. International Electrotechnical Commission, Jun. 2008, vol. IEC 60404-2.

[5] Z.-Q. Zhu, S. Xue, W. Chu, J. Feng, S. Guo, Z. Chen, and J. Peng, "Evaluation of Iron Loss Models in Electrical Machines," *IEEE Transactions on Industry Applications*, vol. 55, no. 2, pp. 1461–1472, Mar. 2019.

[6] J. Li, T. Abdallah, and C. Sullivan, "Improved calculation of core loss with nonsinusoidal waveforms," in *Conference Record of the 2001 IEEE Industry Applications Conference. 36th IAS Annual Meeting (Cat. No.01CH37248)*, vol. 4, Sep. 2001, pp. 2203–2210 vol.4, iSSN: 0197-2618.

[7] K. Venkatachalam, C. Sullivan, T. Abdallah, and H. Tacca, "Accurate prediction of ferrite core loss with nonsinusoidal waveforms using only Steinmetz parameters," in *2002 IEEE Workshop on Computers in Power Electronics, 2002. Proceedings.*, Jun. 2002, pp. 36–41, iSSN: 1093-5142.

[8] D. Lin, P. Zhou, W. Fu, Z. Badics, and Z. Cendes, "A dynamic core loss model for soft ferromagnetic and power ferrite materials in transient finite element analysis," *IEEE Transactions on Magnetics*, vol. 40, no. 2, pp. 1318–1321, Mar. 2004.

[9] K. Yamazaki, Y. Sato, and K. Terauchi, "Loss Analysis of Induction Motors Fed by Inverters by Using Simple Models of Major and Minor Hysteresis Loops in Stator and Rotor Cores," in *2021 IEEE Energy Conversion Congress and Exposition (ECCE)*, Oct. 2021, pp. 4135–4141, iSSN: 2329-3748.

[10] C. Simao, N. Sadowski, N. J. Batistela, and J. P. A. Bastos, "Evaluation of Hysteresis Losses in Iron Sheets Under DC-biased Inductions," *IEEE Transactions on Magnetics*, vol. 45, no. 3, pp. 1158–1161, Mar. 2009.

[11] N. M'zali, F. Martin, U. Aydin, A. Belahcen, A. Benabou, and T. Henneron, "Determination of stress dependent magnetostriction from a macroscopic magneto-mechanical model and experimental magnetization curves," *Journal of Magnetism and Magnetic Materials*, vol. 500, p. 166299, Apr. 2020.

[12] K. Yamazaki and H. Takeuchi, "Impact of Mechanical Stress on Characteristics of Interior Permanent Magnet Synchronous Motors," *IEEE Transactions on Industry Applications*, vol. 53, no. 2, pp. 963–970, Mar. 2017.

[13] A. Krings, "Iron Losses in Electrical Machines - Influence of Material Properties, Manufacturing Processes, and Inverter Operation," 2014. [Online]. Available: https://urn.kb.se/resolve?urn=urn:nbn:se:kth:diva-145243

[14] K. Yamazaki, Y. Togashi, T. Ikemi, S. Ohki, and R. Mizokami, "Reduction of Inverter Carrier Harmonic Losses in Interior Permanent Magnet Synchronous Motors by Optimizing Rotor and Stator Shapes," *IEEE Transactions on Industry Applications*, vol. 55, no. 1, pp. 306–315, Jan. 2019.

[15] F. Stella, E. Vico, D. Cittanti, C. Liu, J. Shen, and R. Bojoi, "Design and Testing of an Automotive Compliant 800V 550 kVA SiC Traction Inverter with Full-Ceramic DC-Link and EMI Filter," in *2022 IEEE Energy Conversion Congress and Exposition (ECCE)*. Detroit, MI, USA: IEEE, Oct. 2022, pp. 1–8.

[16] S. Ferrari, P. Ragazzo, G. Dilevrano, and G. Pellegrino, "Flux and Loss Map Based Evaluation of the Efficiency Map of Synchronous Machines," *IEEE Transactions on Industry Applications*, vol. 59, no. 2, pp. 1500–1509, Mar. 2023.

[17] X. Chen, G. W. Jewell, J. D. Ede, and H. Wu, "Impact of compressive mechanical stress from shrink fitting of a casing on the core loss in a Cobalt Iron stator core of a permanent magnet synchronous machine," in *11th International Conference on Power Electronics, Machines and Drives (PEMD 2022)*. Hybrid Conference, Newcastle, UK: Institution of Engineering and Technology, 2022, pp. 685–691.

[18] A. Varatharajan, D. Brunelli, S. Ferrari, P. Pescetto, and G. Pellegrino, "syreDrive: Automated Sensorless Control Code Generation for Synchronous Reluctance Motor Drives," in *2021 IEEE Workshop on Electrical Machines Design, Control and Diagnosis (WEMDCD)*. Modena, Italy: IEEE, Apr. 2021, pp. 192–197.